THE JOURNAL OF PHYSICAL CHEMISTRY Letters

Letter

Cite This: J. Phys. Chem. Lett. 2019, 10, 4229−4236

pubs.acs.org/JPCL

Quasi-Resonance Fluorine-19 Signal Amplification by Reversible Exchange

Nuwandi M. Ariyasingha,[†] Jacob R. Lindale,[‡] Shannon L. Eriksson,[‡,§] Grayson P. Clark,[∥] Thomas Theis,[⊥] Roman V. Shchepin,[#] Nikita V. Chukanov,[▽,○] Kirill V. Kovtunov,[▽,○] Igor V. Koptyug,[▽,○] Warren S. Warren,[◆] and Eduard Y. Chekmenev*[,†,¶]

[†]Department of Chemistry, Integrative Biosciences (Ibio), Wayne State University, Karmanos Cancer Institute (KCI), Detroit, Michigan 48202, United States

[‡]Department of Chemistry, Duke University, Durham, North Carolina 27708, United States

[§]School of Medicine, Duke University, Durham, North Carolina 27708, United States

[∥]Department of Biomedical Engineering, Duke University, Durham, North Carolina 27708, United States

[⊥]Department of Chemistry, North Carolina State University, Raleigh, North Carolina 27695-8204, United States

[#]Department of Chemistry and Applied Biological Sciences, South Dakota School of Mines and Technology, Rapid City, South Dakota 57701, United States

[▽]International Tomography Center, SB RAS, 3A Institutskaya St., Novosibirsk 630090, Russia

[○]Novosibirsk State University, 2 Pirogova St., Novosibirsk 630090, Russia

[◆]Departments of Physics, Chemistry, Biomedical Engineering, and Radiology, Duke University, Durham, North Carolina 27708, United States

[¶]Russian Academy of Sciences, Leninskiy Prospekt 14, Moscow, 119991, Russia

Supporting Information

ABSTRACT: We report on an extension of the quasi-resonance (QUASR) pulse sequence used for signal amplification by reversible exchange (SABRE), showing that we may target distantly *J*-coupled ^{19}F-spins. Polarization transfer from the parahydrogen-derived hydrides to the ^{19}F nucleus is accomplished via weak five-bond *J*-couplings using a shaped QUASR radio frequency pulse at a 0.05 T magnetic field. The net result is the direct generation of hyperpolarized ^{19}F *z*-magnetization, derived from the parahydrogen singlet order. An accumulation of ^{19}F polarization on the free ligand is achieved with subsequent repetition of this pulse sequence. The hyperpolarized ^{19}F signal exhibits clear dependence on the pulse length, irradiation frequency, and delay time in a manner similar to that reported for ^{15}N QUASR-SABRE. Moreover, the hyperpolarized ^{19}F signals of 3-^{19}F-^{14}N-pyridine and 3-^{19}F-^{15}N-pyridine isotopologues are similar, suggesting that (i) polarization transfer via QUASR-SABRE is irrespective of the nitrogen isotopologue and (ii) the presence or absence of the spin-1/2 ^{15}N nucleus has no impact on the efficiency of QUASR-SABRE polarization transfer. Although optimization of polarization transfer efficiency to ^{19}F ($P_{^{19}F} \approx 0.1\%$) was not the goal of this study, we show that high-field SABRE can be efficient and broadly applicable for direct hyperpolarization of ^{19}F spins.

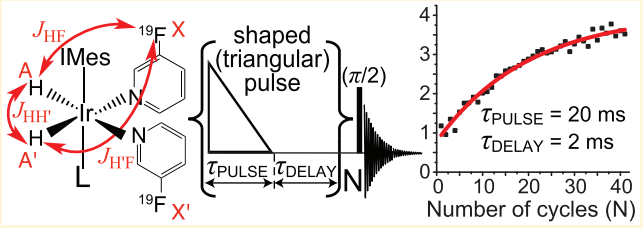

Hyperpolarization techniques increase nuclear spin polarization (*P*) by several orders of magnitude, enabling the corresponding gains in signals over that attainable via conventional NMR spectroscopy and MRI.[1−4] This revolutionary boost in detection sensitivity enables new applications such as detection of dilute biologically relevant molecules both in vitro[5−7] and in vivo.[8−12] A particularly exciting hyperpolarization technique is signal amplification by reversible exchange (SABRE), pioneered by Duckett and co-workers.[13−17] SABRE relies on simultaneous chemical exchange of parahydrogen (p-H_2) and substrate targeted for hyperpolarization (S) with an iridium polarization transfer catalyst (PTC), Figure 1a, during which the singlet order from the p-H_2-derived hydrides is allowed to transfer to the nuclear spins of the target substrates via the network of *J*-couplings. SABRE has gained popularity[18] because it is fast, efficient, and inexpensive relative to competing techniques. Polarization transfer is frequently accomplished in less than a minute with polarizations *P* sometimes exceeding 30%,[19−21] at a cost several orders of magnitude smaller than that of dissolution dynamic

Received: May 25, 2019
Accepted: July 10, 2019
Published: July 10, 2019

DOI: 10.1021/acs.jpclett.9b01505
J. Phys. Chem. Lett. 2019, 10, 4229−4236

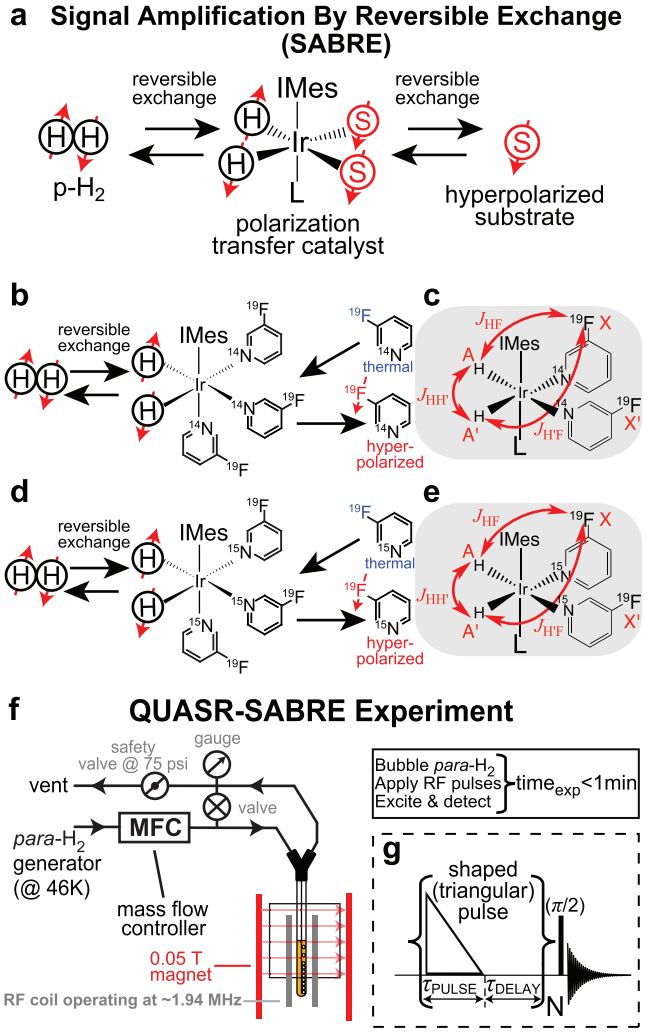

Figure 1. (a) Schematic of simultaneous chemical exchange of parahydrogen (p-H_2) and target substrate (S) on an activated IrIMes PTC in SABRE hyperpolarization process. (b) Schematic of SABRE chemical exchange with 3-^{19}F-pyridine as a substrate. (c) Spin system formed on the IrIMes catalyst with 3-^{19}F-pyridine as a substrate. (d) Schematic of SABRE chemical exchange with 3-^{19}F-^{15}N-pyridine as a substrate. (e) Spin system formed on the IrIMes catalyst with 3-^{19}F-^{15}N-pyridine as a substrate. Note the difference between the spin systems shown in panels c and e due to the presence of ^{14}N (natural abundance) and ^{15}N (isotopically enriched) nuclei. It is important to note that $^{5}J_{FH} \neq {}^{5}J_{FH'}$ in both panels c and e. (f) Schematic of the experimental setup for ^{19}F QUASR-SABRE experiment. (g) Overall schematic for quasi-resonance SABRE RF pulsing.

nuclear polarization (d-DNP), an alternative method of hyperpolarization.[4,22]

There are two major approaches for polarization transfer in SABRE. The first approach is conventional SABRE, which relies on coherently driven dynamics generated at a level anticrossing (LACs).[23,24] The LAC condition is achieved by matching a static magnetic field to the resonance frequency of the singlet to target magnetization transition, allowing flow of spin order through J-couplings of nuclear spins involved in the polarization transfer.[13] For the homonuclear case of conventional SABRE, as in polarization transfer from p-H_2-derived hydrides to the protons on the target substrate, the LAC condition is met at a magnetic field of a few millitesla and is determined by the chemical shift difference between p-H_2-derived hydrides and the target protons. For the heteronuclear case of conventional SABRE, broadly referring to polarization transfer from p-H_2-derived hydrides to the substrate's ^{13}C,[25] ^{15}N,[26] ^{31}P,[27] etc., the LAC condition is met at a magnetic field of a few microtesla,[26,28−30] determined by the difference in gyromagnetic ratios of the proton and target nucleus. The second approach to polarization transfer relies on application of radio frequency (RF) pulses, which are employed to create LAC conditions in an arbitrarily high magnetic field, e.g., the low-irradiation generation of high tesla-SABRE (LIGHT-SABRE) pulse sequence.[31] A number of other approaches have been demonstrated over the years, such as RF-SABRE,[32] spin-lock induced crossing-SABRE (SLIC-SABRE),[33] delayed adiabatic ramps transfer hyperpolarization-SABRE (DARTH-SABRE),[34] and others.[35,36] One key strength of the RF-based approach, which has remained largely unrealized, is the potential to perform SABRE at a wide range of magnetic fields. For example, one can use low-field, and potentially portable, electromagnets; high-resolution NMR spectrometers; or MRI scanners. The RF-based approaches have primarily focused on SABRE of ^{15}N spins for two reasons: First, the dipolar relaxation of ^{15}N magnetization is significantly longer and there is great potential for extremely long-lived ($T_s \approx 20$ min) $^{15}N_2$ singlet states.[37−43] Second, isotopic enrichment of ^{15}N heterocycles[44−46] and other molecular carriers that efficiently bind iridium is relatively simple.[45,47]

SABRE hyperpolarization of ^{19}F spins is particularly attractive, because the ^{19}F spin has the second highest detection sensitivity among stable nuclei with a gyromagnetic ratio ($\gamma_{^{19}F}$) of 0.93·$\gamma_{^{1}H}$, and approximately 9·$\gamma_{^{15}N}$. Moreover, unlike ^{15}N and ^{13}C, ^{19}F is nearly 100% naturally abundant, obviating the need for isotopic enrichment needed for ^{15}N- and ^{13}C-labeled targets. While ^{19}F is found in more than 20% of drugs,[48,49] it has a negligible biological presence, making its spectroscopic and imaging detection relatively background-free compared to that of proton spins. This allows the potential for broad applications for the theranostic imaging and studies of drug interactions. To the best of our knowledge, there have been five previous reports on SABRE hyperpolarization of ^{19}F using spontaneous polarization transfer and no reported efforts using an RF-based SABRE approach.[13,50−53] In this work, we employ a recently developed QUASi-Resonance SABRE[54] (QUASR-SABRE) experiment, relying on SLIC pulses,[55] for feasibility studies of RF-based hyperpolarization of ^{19}F spins five bonds removed from the p-H_2-derived hydrides.

For this study, we have used two compounds as SABRE substrates: 3-^{19}F-pyridine (196665, Sigma-Aldrich) and recently synthesized 3-^{19}F-^{15}N-pyridine,[51] seen in panels b and d of Figure 1, respectively. Panels c and e of Figure 1 show the network of J-couplings formed during the temporary association of p-H_2 and the corresponding target substrates with an activated precatalyst [Ir(IMes)(COD)Cl] (IMes = 1,3-bis(2,4,6-trimethylphenyl)imidazol-2-ylidene, COD = 1,5-cyclooctadiene).[17] A solution of 100 mM substrates (3-^{19}F-pyridine or 3-^{19}F-^{15}N-pyridine) and 5 mM IrIMes[17] catalyst was prepared in methanol-d_4 and activated for at least 30 min with pH_2 flow of 20 standard cubic centimeters (sccm) . Approximately 87% pH_2 was directed into a medium-walled 5 mm NMR tube setup at a flow rate of ∼70 sccm while the QUASR-SABRE pulse sequence was applied (Figure 1g).

We have employed three different ^{19}F hyperpolarization approaches: (i) QUASR-SABRE; (ii) in situ SABRE, the

DOI: 10.1021/acs.jpclett.9b01505
J. Phys. Chem. Lett. 2019, 10, 4229−4236

process of hyperpolarization by applying a 90-degree hard pulse during p-H_2 bubbling at the spectrometer field (0.05 T); and (iii) conventional SABRE at 6 mT.[13,55] The QUASR-SABRE study of 3-^{19}F-pyridine and 3-^{19}F-^{15}N-pyridine was performed using a 0.05 T NMR spectrometer under similar experimental conditions[54] but with the spectrometer operating at the ^{19}F Larmor frequency (1.94 MHz). The shaped pulse was applied with a maximum ω_1 = 1.24 kHz and a ramp down to ω_1 = 0 Hz for τ_{PULSE}, followed by a subsequent inter-pulse delay τ_{DELAY} (Figure 1f). Given significant nonlinearities in the low-power range of the radio frequency (RF) amplifier, the actual applied pulse can be closely approximated with a truncated double-Gaussian pulse of the form

$$s(t) = \frac{1}{2}(a_1 e^{-t^2/\tau_{PULSE}^2\cdot\sigma_1} + a_2 e^{-t^2/\tau_{PULSE}^2\cdot\sigma_2}) \left(1 - \tanh\left(\frac{t}{\tau_{PULSE}\cdot\delta} - a_3\right)\right) \quad (1)$$

The values for each of the variables in eq 1 are given in the Supporting Information. This QUASR-SABRE pulse sequence has the potential to be applied without modifications dependent on molecular parameters, like the magnitude of the J-couplings or chemical shifts. The large pulse power and ramped pulse shape make hyperpolarization insensitive to the frequency offset despite pumping the LAC far from the optimal resonance condition. The process of pulsing and delay was repeated N times before irradiating the sample with a hard 90-pulse similar to previous work,[54] and the free induction decay was detected (Figure 1g).

Recently, a quantum Monte Carlo (QMC) simulation approach to SABRE dynamics was introduced,[38] which demonstrated the ability to predict coherent hyperpolarization dynamics for pulsed SABRE experiments with high accuracy. However, this method would have a prohibitive computational cost in the limit where there is a significant degree of coupling between each pulse, like the case here, as the entire pulse-train must be simulated. So long as the time-step of the simulation is much smaller than the lifetime of the SABRE complex τ_{PTC}, the coherent hyperpolarization dynamics are well-approximated by

$$\partial_t\hat{\rho} = -i[\hat{H}, \hat{\rho}] - \frac{\hat{M}\hat{\rho}}{\tau_{PTC}} \quad (2)$$

where $\hat{M}$ is the same operator to control exchange as used in the QMC simulation. The approximation made by eq 2 has the distinct advantage that it has a simple numerical solution that does not require iteration, making the simulation incredibly fast. This makes the explicit calculation of the effects of entire pulse sequences tractable, as opposed to approximating the dynamics as being identical and additive under each pulse, as done previously. In the simulations shown here, we have used a 10 μs step size and have approximated the $\tau_{PTC} \approx 25$ ms. We note that this spin system is at the upper computational limit for Liouville space; however, it is far from the 15-spin limit of the Hilbert-space methods utilized here.

Specifically, we have constructed this system to include the parahydrogen-derived hydrides, the long-range ^{19}F nuclei, and ortho-protons on pyridine, as it is assumed that all other couplings are either small or will not significantly affect the ^{19}F hyperpolarization dynamics. This forms a six-spin AA′(BX)-(B′X′) system with the Hamiltonian:

$$\hat{H}(t) = \sum_i \Delta\omega_i\hat{I}_{iz} + \Delta\omega_F(\hat{S}_{4z} + \hat{S}_{6z}) + 2\pi\begin{bmatrix} J_{HH}\hat{I}_1\cdot\hat{I}_2 + J_{HH'}(\hat{I}_{1z}\hat{I}_{3z} + \hat{I}_{2z}\hat{I}_{5z}) + \\ J_{HF}(\hat{I}_{1z}\hat{S}_{4z} + \hat{I}_{2z}\hat{S}_{6z}) + J_{H'F}(\hat{I}_{3z}\hat{S}_{4z} + \hat{I}_{5z}\hat{S}_{6z}) \end{bmatrix} + \omega_{1F}(t)(\hat{S}_{4x} + \hat{S}_{6x}) \quad (3)$$

The $J_{HH'}$ term is the coupling between the hydrides on the ortho-proton, J_{HF} the long-range $^5J_{HF}$ coupling, $J_{H'F}$ the ortho-proton to ^{19}F ^3J-coupling, and $\omega_{1F}(t)$ the time-dependent pulse shape in the case of the QUASR-SABRE pulse sequence.

The ^{19}F QUASR-SABRE spectra of 3-^{19}F-pyridine and 3-^{19}F-^{15}N-pyridine are shown in panels a and b of Figure 2, respectively, exhibiting $\varepsilon^{19}_F \approx 6700$ ($P_F \approx 0.10\%$) and $\varepsilon^{19}_F \approx 7100$ ($P_F \approx 0.11\%$), respectively. Conventional SABRE yielded an $\varepsilon_F \approx 17\,800$ ($P_F \approx 0.26\%$) for 3-^{19}F-^{15}N-pyridine, shown in Figure 2f, which is highly surprising as there are no resonance conditions at 6 mT that lead to hyperpolarized fluorine magnetization. The resonance condition for ^{19}F hyperpolariza-

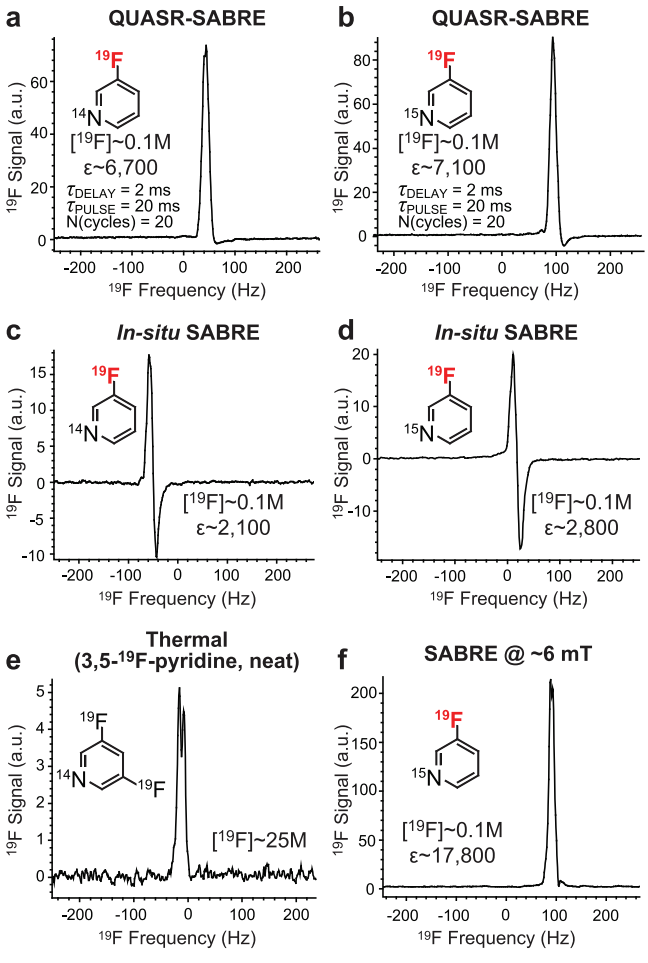

Figure 2. ^{19}F spectra of QUASR-SABRE hyperpolarized 3-^{19}F-pyridine (a) and of QUASR-SABRE hyperpolarized 3-^{19}F-^{15}N-pyridine (b). ^{19}F in situ SABRE spectra of hyperpolarized 3-^{19}F-pyridine (c) and 3-^{19}F-^{15}N-pyridine (d). Note that although the signals are hyperpolarized, the NMR lines are antiphase, which may not be suitable for some MRI sequences. ^{19}F spectrum of thermally polarized signal reference neat 3,5-^{19}F-pyridine (e). ^{19}F spectrum of 3-^{19}F-^{15}N-pyridine hyperpolarized via conventional SABRE at ~6 mT (f). All NMR spectra were acquired using a single scan.

DOI: 10.1021/acs.jpclett.9b01505
J. Phys. Chem. Lett. 2019, 10, 4229−4236

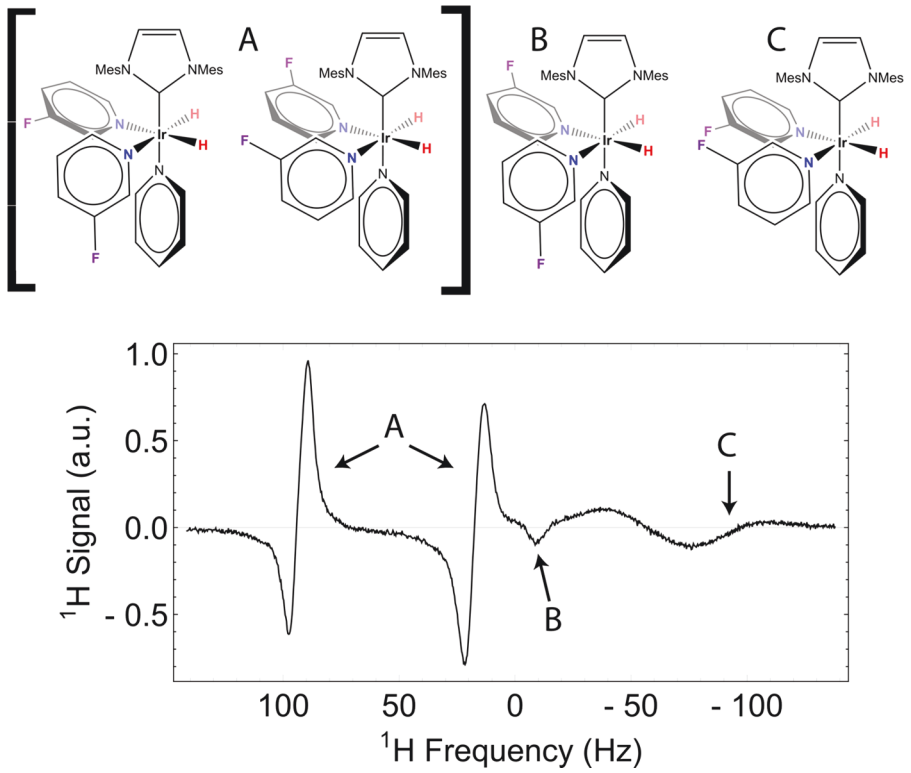

Figure 3. (top) Conformers of the activated PTC with associated ligands and hydrides inducing different chemical environments for the associated hydrides. (bottom) ^{1}H spectrum at 1 T with 45° tip angle demonstrating four distinct hydride species coming from three inequivalent conformers with two pairs of equivalent hydrides (B and C) and one pair of inequivalent hydrides (A).

tion is instead at approximately ±3.2 μT. This suggests that the resulting ^{19}F-signal arises from cross relaxation from the ortho-^{1}H on the pyridinyl ring.[51] Spectra acquired with either QUASR-SABRE or conventional SABRE exhibit in-phase resonances in contrast to the in situ SABRE spectra of the corresponding compounds (Figure 2c,d), which exhibit antiphase spin order. This antiphase spin order arises as, in the absence of a radiofrequency pulse, there is still an allowed transition between the $S_H T^0_{H'F_z} \rightarrow T^0_H S_{H'F}$ states, for which the $S_{H'F}$ order rapidly decays into $\hat{I}_{H'z}\hat{S}_{Fz}$ because of the ∼120 kHz frequency difference between the ^{1}H and ^{19}F nuclei at this field. Conversely, off-resonance SLIC excitation is known to generate solely in-phase $\hat{S}_z$ order, as will any hyperpolarized signal derived from cross relaxation from the ortho-^{1}H. Note that the frequency shift observed in all the spectra shown in Figure 2 is a result of the magnetic field drift due to the temperature fluctuations of the B_0 magnet occurring during the spectral acquisition process.

The spectra shown in Figure 2a,b suggest that the observed signals are the result of direct polarization transfer from the *p*-H_2-derived hydrides to ^{19}F nuclei driven by QUASR-SABRE. This is because the observed spectra have in-phase signatures, versus the antiphase signatures expected from in situ hyperpolarization (Figure 2c,d), and no ortho-^{1}H magnetization is generated at this field to afford cross relaxation. Moreover, we do not expect the spin-1/2 relayed mechanism through $^2J_{NH}$ to be the dominant pathway for hyperpolarization transfer, because there is little difference in the SABRE spectra of 3-^{19}F-pyridine and 3-^{19}F-^{15}N-pyridine.[21,56]

The enhancement values were computed as described previously[54] by taking the product of the ratio of the ^{19}F concentrations of the species of interest (C_{REF}/C_{HP}), i.e., ^{19}F, present in the thermally polarized reference compound (C_{REF}, neat 3,5-^{19}F-pyridine; Figure 2e) and the HP substrate compound (C_{HP}), with the integrated signal intensity ratio of the HP substrate and the thermal signal reference compound (S_{HP}/S_{REF}) multiplied by a factor of 1.85 (which is the ratio of the cross-sectional areas of the thermal signal reference to the hyperpolarized arrangements as implemented by the experimental setup) as discussed in detail elsewhere.[57] Nuclear spin polarization P was computed by multiplying $\varepsilon_{^{19}F}$ by equilibrium ^{19}F polarization at 0.05 T and 300 K (ca. 1.5×10^{-5}%).

3-^{19}F-Pyridine presents an interesting chemical system, as the complex may take on four possible conformations upon association of two 3-^{19}F-pyridine ligands as seen in Figure 3. When the fluorine substituents are both positioned between the pyridine rings, the complex is highly unstable because of the proximity of two highly electronegative groups. The hydrides in this conformer are therefore short-lived and yield the broad peak labeled "C" in Figure 3. When the fluorine substituents are both positioned in the periphery, the complex is stable and yields a longer-lived hydride species producing the peak labeled "B". The two conformers with one central and one peripheral fluorine substituent are degenerate and are not destabilized by proximity of the fluorine substituents. Because the meta-substituted pyridine is asymmetric, this final conformation induces a chemical inequivalence between the hydrides producing two antisymmetric peaks labeled "A" separated by 1.77 ppm. This chemical shift difference prevents LIGHT-SABRE[31] hyperpolarization at high field. However, using a lower field (50 mT) as in QUASR-SABRE allows collapse of these disparate hydride resonance frequencies onto a single peak of accidental equivalence.

DOI: 10.1021/acs.jpclett.9b01505
J. Phys. Chem. Lett. 2019, 10, 4229−4236

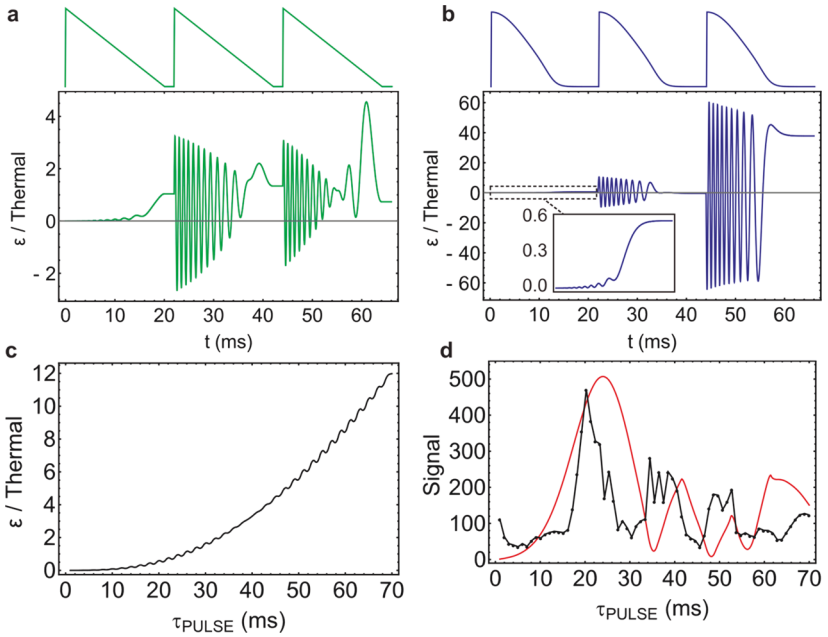

Figure 4. ^{19}F QUASR-SABRE of 3-^{19}F-pyridine. Coherent hyperpolarization dynamics during a triangular pulse (a) and the nonlinear pulse approximation used in these experiments (b). The dynamics predicted during a single pulse (c) vary greatly from those predicted from the explicit calculation of the entire pulse sequence (d), which is shown in red overlaying the experimental (0.05 T) data in black (the black solid lines are added to guide the eye).

The QUASR-SABRE pulse sequence was applied in a regime where there is extreme coherent coupling between each consecutive QUASR pulse, which arises when the delay is much shorter than the lifetime of the species (typically ∼25 ms). In such a regime, the dynamics generated by the pulse sequence are far from intuitive. Given that the ortho-protons of the pyridine are ∼100 Hz offset in resonance from the parahydrogen-derived hydrides, this spin system effectively reduces to an AA′XX′ spin system, for which the SABRE dynamics have been characterized extensively.[35] During the first pulse, very little hyperpolarized signal is generated until the pulse power approaches the LAC condition, given by $\omega_{1F}/2\pi = {}^2J_{HH}$. Given the short 2 ms interpulse delay, the beginning of each subsequent QUASR pulse induces large coherent oscillations at the, albeit time-dependent, nutation frequency. The relatively large signal produced with a (20 ms QUASR-pulse +2 ms delay)$_{30}$ train corresponds to when the coherent oscillations halt coincident with an effective $(2n + 1)\pi$-pulse in the hyperpolarization dynamics, giving the largest deviation from equilibrium. The optimal 2 ms delay was surprising, given that other pulsed techniques[34] find the optimal interpulse delay at times on the order of 100 ms. However, given that the QUASR-pulse power is so off-resonance from the SLIC matching condition, only a small amount of polarization may be generated from each pulse; thus, not requiring significant parahydrogen exchange, the interpulse delay can be largely decreased to afford larger signals in this experiment. Interestingly, the maximum observed in Figure 4c is recovered only when the nonlinearities in the pulse shape are reintroduced into the simulation.

It is important to note that the QUASR-SABRE signals are approximately 2.6-fold smaller than the signal obtained by conventional SABRE (Figure 2). This is well understood as the ramifications of various experimental details. First, because the rapid coherent oscillations induced by the QUASR-pulse will average under exchange toward the center of these oscillations, the hyperpolarization generated by each pulse is significantly damped. Also, the large nutation frequency allows for simultaneous irradiation of the free ^{19}F-species, thus dramatically attenuating the signal to 52% of the generated hyperpolarization (see the Supporting Information for details). Given that $^5J_{HF}$ = 0.34 Hz,[58] only small perturbations can be made to the system, leading to very slow oscillations on the order of seconds, with very weak pulses, on the order of a few hertz in amplitude, as detailed by conventional SLIC theory.[31,59] Despite the experimental limitations of the complex polarization dynamics, our key finding of the feasibility of QUASR-SABRE polarization of ^{19}F is extended by the insensitivity of the hyperpolarized ^{19}F signal to the frequency offset (Figure 5a), showing that even with a ∼300 Hz offset significant polarization may be achieved. Naturally, the hyperpolarized ^{19}F signal increases with N pumping cycles, demonstrating a clear polarization build-up (Figure 5b) in a manner consistent with SABRE.[31,54] Note the positive value at

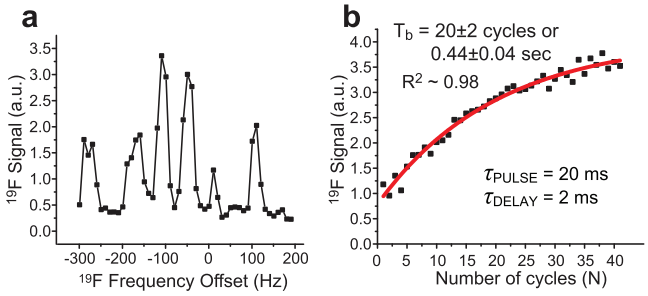

Figure 5. ^{19}F QUASR-SABRE of 3-^{19}F-pyridine. Hyperpolarized 3-^{19}F-pyridine signal dependence on the SLIC-pulse frequency offset (a) and number of pumping cycles (N) demonstrating the build-up of ^{19}F polarization with the monoexponential build-up (red curve) constant of 0.44 ± 0.04 s (b). All data were acquired at 0.05 T magnetic field, and the black solid lines are added to guide the eye.

DOI: 10.1021/acs.jpclett.9b01505
J. Phys. Chem. Lett. 2019, 10, 4229−4236

$N = 0$ is likely due to residual polarization build-up due to in situ SABRE.

We have shown that fluorine hyperpolarization can be generated directly through five chemical bonds with the QUASR-SABRE experiment, which is significantly further than with nearly all other reported approaches for SABRE. The ^{19}F polarization levels achieved by the QUASR-SABRE approach here are relatively low (ca. 0.1%), although fundamentally significantly higher polarization levels should be achievable, i.e. potentially significantly exceeding 10%, and it is important to discuss the areas of potential improvement of the QUASR-SABRE approach. First and foremost, the applications of RF pulses need to be better synchronized with/tailored to the exchange processes, and issues with nonlinear polarization dynamics (which significantly decreased the attainable polarization level in this study, see the Supporting Information for details) may potentially improve the polarization transfer efficiency by several folds. Second, the use of higher and more homogeneous magnetic fields may render the opportunity to more selectively excite catalyst-bound ^{19}F resonance, while having less destructive effect on ^{19}F resonances of free species. Third, the design of more advanced shapes of the RF pulse with optimized RF power may also significantly boost the efficiency of the QUASR-SABRE approach. Moreover, the additional improvement in operation conditions, such as increasing pH_2 pressure, parahydrogen fraction, and pH_2 flow rate, will likely also improve the overall level of ^{19}F polarization. Although biomedical applications such as ^{19}F-based in vivo tracking, spectroscopy, or imaging will be challenging to perform with the relatively low polarization level of ^{19}F polarization, future improvements (as described above) may likely enable such applications in a manner similar to that of biomedical applications of ^{13}C HP contrast agents. We hope the pioneering results reported here can be improved and that higher levels of ^{19}F polarization can be obtained through future work across a wide range of compounds such as ^{19}F-containing drugs with suitable *N*-heterocyclic motifs (e.g., 5-fluorouracil, celecoxib, sitagliptin, fluconazole, etc.). We note that not any ^{19}F-containing molecule can be readily hyperpolarized via SABRE in general and the QUASR-SABRE approach in particular, because of the requirement of chemical exchange of ^{19}F-containing molecules on a suitable time scale (0.001−0.1 s). While currently the SABRE hyperpolarization approach has been broadly applied to N-containing heterocycles, the chemistry of SABRE-amenable biomolecular motifs is rapidly growing because of new chemistries of exchange, which has recently made S-heterocycles[60] and keto-carboxylic acids[61] amenable to SABRE hyperpolarization. As the SABRE hyperpolarization technique continues to rapidly develop, we expect more biomolecular structures (including drugs) to be amenable to QUASR-SABRE hyperpolarization. Spectroscopy of ^{19}F-hyperpolarized drugs is attractive because the lack of background signal and greater chemical shift dispersion of ^{19}F compared to that of ^{1}H allow for specific characterization with little to no background interference. Moreover, RF-based hyperpolarization approaches offer many practical advantages compared to low-field methods as the sample does not need to be shuttled between the matching field and the detector field, therefore enabling signal averaging and multidimensional HP NMR spectroscopy.[62]

■ ASSOCIATED CONTENT

Supporting Information

The Supporting Information is available free of charge on the ACS Publications website at DOI: 10.1021/acs.jpclett.9b01505.

^{19}F QUASR-SABRE simulation description; Mathematica code (PDF)

■ AUTHOR INFORMATION

Corresponding Author

*E-mail: chekmenev@wayne.edu.

ORCID

Thomas Theis: 0000-0001-6779-9978
Kirill V. Kovtunov: 0000-0001-7577-9619
Igor V. Koptyug: 0000-0003-3480-7649
Warren S. Warren: 0000-0001-8458-2076
Eduard Y. Chekmenev: 0000-0002-8745-8801

Notes

The authors declare no competing financial interest.

■ ACKNOWLEDGMENTS

This work was supported by NSF under Grants CHE-1836308 and CHE-1665090. Research reported in this publication was also supported by the National Institute of Biomedical Imaging and Bioengineering of the NIH under R21EB025313, and 1R21EB020323; by National Cancer Institute under 1R21CA220137; and by DOD CDMRP under BRP W81XWH-12-1-0159/BC112431 and under W81XWH-15-1-0271. Russian team thanks grants from RFBR (17-54-33037, 18-43-543023, 19-43-540004) and Higher Education of the RF (AAAA-A16-116121510087-5).

■ REFERENCES

(1) Goodson, B. M.; Whiting, N.; Coffey, A. M.; Nikolaou, P.; Shi, F.; Gust, B. M.; Gemeinhardt, M. E.; Shchepin, R. V.; Skinner, J. G.; Birchall, J. R.; et al. Hyperpolarization Methods for MRS. *Emagres* **2015**, *4*, 797−810.

(2) Nikolaou, P.; Goodson, B. M.; Chekmenev, E. Y. NMR Hyperpolarization Techniques for Biomedicine. *Chem. - Eur. J.* **2015**, *21*, 3156−3166.

(3) Kovtunov, K. V.; Pokochueva, E. V.; Salnikov, O. G.; Cousin, S.; Kurzbach, D.; Vuichoud, B.; Jannin, S.; Chekmenev, E. Y.; Goodson, B. M.; Barskiy, D. A.; et al. Hyperpolarized NMR: D-DNP, PHIP, and SABRE. *Chem. - Asian J.* **2018**, *13*, 1857−1871.

(4) Ardenkjaer-Larsen, J. H.; Fridlund, B.; Gram, A.; Hansson, G.; Hansson, L.; Lerche, M. H.; Servin, R.; Thaning, M.; Golman, K. Increase in Signal-to-Noise Ratio of > 10,000 Times in Liquid-State NMR. *Proc. Natl. Acad. Sci. U. S. A.* **2003**, *100*, 10158−10163.

(5) Eshuis, N.; van Weerdenburg, B. J. A.; Feiters, M. C.; Rutjes, F. P. J. T.; Wijmenga, S. S.; Tessari, M. Quantitative Trace Analysis of Complex Mixtures Using SABRE Hyperpolarization. *Angew. Chem., Int. Ed.* **2015**, *54*, 1481−1484.

(6) Reile, I.; Aspers, R. L. E. G.; Tyburn, J.-M.; Kempf, J. G.; Feiters, M. C.; Rutjes, F. P. J. T.; Tessari, M. Dosy Analysis of Micromolar Analytes: Resolving Dilute Mixtures by SABRE Hyperpolarization. *Angew. Chem., Int. Ed.* **2017**, *56*, 9174−9177.

(7) Barskiy, D. A.; Coffey, A. M.; Nikolaou, P.; Mikhaylov, D. M.; Goodson, B. M.; Branca, R. T.; Lu, G. J.; Shapiro, M. G.; Telkki, V.-V.; Zhivonitko, V. V.; et al. NMR Hyperpolarization Techniques of Gases. *Chem. - Eur. J.* **2017**, *23*, 725−751.

(8) Kurhanewicz, J.; Vigneron, D. B.; Brindle, K.; Chekmenev, E. Y.; Comment, A.; Cunningham, C. H.; DeBerardinis, R. J.; Green, G. G.; Leach, M. O.; Rajan, S. S.; et al. Analysis of Cancer Metabolism by

DOI: 10.1021/acs.jpclett.9b01505
J. Phys. Chem. Lett. 2019, 10, 4229−4236

Imaging Hyperpolarized Nuclei: Prospects for Translation to Clinical Research. *Neoplasia* **2011**, *13*, 81−97.
(9) Nelson, S. J.; Kurhanewicz, J.; Vigneron, D. B.; Larson, P. E. Z.; Harzstark, A. L.; Ferrone, M.; van Criekinge, M.; Chang, J. W.; Bok, R.; Park, I.; et al. Metabolic Imaging of Patients with Prostate Cancer Using Hyperpolarized 1-C-13 Pyruvate. *Sci. Transl. Med.* **2013**, *5*, 198ra108.
(10) Hövener, J.-B.; Pravdivtsev, A. N.; Kidd, B.; Bowers, C. R.; Glöggler, S.; Kovtunov, K. V.; Plaumann, M.; Katz-Brull, R.; Buckenmaier, K.; Jerschow, A.; et al. Parahydrogen-Based Hyperpolarization for Biomedicine. *Angew. Chem., Int. Ed.* **2018**, *57*, 11140−11162.
(11) Golman, K.; in 't Zandt, R.; Thaning, M. Real-Time Metabolic Imaging. *Proc. Natl. Acad. Sci. U. S. A.* **2006**, *103*, 11270−11275.
(12) Day, S. E.; Kettunen, M. I.; Gallagher, F. A.; Hu, D. E.; Lerche, M.; Wolber, J.; Golman, K.; Ardenkjaer-Larsen, J. H.; Brindle, K. M. Detecting Tumor Response to Treatment Using Hyperpolarized C-13 Magnetic Resonance Imaging and Spectroscopy. *Nat. Med.* **2007**, *13*, 1382−1387.
(13) Adams, R. W.; Aguilar, J. A.; Atkinson, K. D.; Cowley, M. J.; Elliott, P. I. P.; Duckett, S. B.; Green, G. G. R.; Khazal, I. G.; Lopez-Serrano, J.; Williamson, D. C. Reversible Interactions with Para-Hydrogen Enhance NMR Sensitivity by Polarization Transfer. *Science* **2009**, *323*, 1708−1711.
(14) Adams, R. W.; Duckett, S. B.; Green, R. A.; Williamson, D. C.; Green, G. G. R. A Theoretical Basis for Spontaneous Polarization Transfer in Non-Hydrogenative Parahydrogen-Induced Polarization. *J. Chem. Phys.* **2009**, *131*, 194505.
(15) Atkinson, K. D.; Cowley, M. J.; Elliott, P. I. P.; Duckett, S. B.; Green, G. G. R.; Lopez-Serrano, J.; Whitwood, A. C. Spontaneous Transfer of Parahydrogen Derived Spin Order to Pyridine at Low Magnetic Field. *J. Am. Chem. Soc.* **2009**, *131*, 13362−13368.
(16) Balu, A. M.; Duckett, S. B.; Luque, R. Para-Hydrogen Induced Polarisation Effects in Liquid Phase Hydrogenations Catalysed by Supported Metal Nanoparticles. *Dalton Trans* **2009**, 5074−5076.
(17) Cowley, M. J.; Adams, R. W.; Atkinson, K. D.; Cockett, M. C. R.; Duckett, S. B.; Green, G. G. R.; Lohman, J. A. B.; Kerssebaum, R.; Kilgour, D.; Mewis, R. E. Iridium N-Heterocyclic Carbene Complexes as Efficient Catalysts for Magnetization Transfer from Para-Hydrogen. *J. Am. Chem. Soc.* **2011**, *133*, 6134−6137.
(18) Colell, J. F. P.; Logan, A. W. J.; Zhou, Z.; Shchepin, R. V.; Barskiy, D. A.; Ortiz, G. X.; Wang, Q.; Malcolmson, S. J.; Chekmenev, E. Y.; Warren, W. S.; et al. Generalizing, Extending, and Maximizing Nitrogen-15 Hyperpolarization Induced by Parahydrogen in Reversible Exchange. *J. Phys. Chem. C* **2017**, *121*, 6626−6634.
(19) Rayner, P. J.; Burns, M. J.; Olaru, A. M.; Norcott, P.; Fekete, M.; Green, G. G. R.; Highton, L. A. R.; Mewis, R. E.; Duckett, S. B. Delivering Strong ^{1}H Nuclear Hyperpolarization Levels and Long Magnetic Lifetimes through Signal Amplification by Reversible Exchange. *Proc. Natl. Acad. Sci. U. S. A.* **2017**, *114*, E3188−E3194.
(20) Kidd, B. E.; Gesiorski, J. L.; Gemeinhardt, M. E.; Shchepin, R. V.; Kovtunov, K. V.; Koptyug, I. V.; Chekmenev, E. Y.; Goodson, B. M. Facile Removal of Homogeneous SABRE Catalysts for Purifying Hyperpolarized Metronidazole, a Potential Hypoxia Sensor. *J. Phys. Chem. C* **2018**, *122*, 16848−16852.
(21) Barskiy, D. A.; Shchepin, R. V.; Coffey, A. M.; Theis, T.; Warren, W. S.; Goodson, B. M.; Chekmenev, E. Y. Over 20% ^{15}N Hyperpolarization in under One Minute for Metronidazole, an Antibiotic and Hypoxia Probe. *J. Am. Chem. Soc.* **2016**, *138*, 8080−8083.
(22) Ardenkjaer-Larsen, J. H. On the Present and Future of Dissolution-DNP. *J. Magn. Reson.* **2016**, *264*, 3−12.
(23) Pravdivtsev, A. N.; Yurkovskaya, A. V.; Vieth, H.-M.; Ivanov, K. L.; Kaptein, R. Level Anti-Crossings Are a Key Factor for Understanding Para-Hydrogen-Induced Hyperpolarization in SABRE Experiments. *ChemPhysChem* **2013**, *14*, 3327−3331.
(24) Ivanov, K. L.; Pravdivtsev, A. N.; Yurkovskaya, A. V.; Vieth, H.-M.; Kaptein, R. The Role of Level Anti-Crossings in Nuclear Spin Hyperpolarization. *Prog. Nucl. Magn. Reson. Spectrosc.* **2014**, *81*, 1−36.
(25) Barskiy, D. A.; Shchepin, R. V.; Tanner, C. P. N.; Colell, J. F. P.; Goodson, B. M.; Theis, T.; Warren, W. S.; Chekmenev, E. Y. The Absence of Quadrupolar Nuclei Facilitates Efficient ^{13}C Hyperpolarization Via Reversible Exchange with Parahydrogen. *ChemPhysChem* **2017**, *18*, 1493−1498.
(26) Theis, T.; Truong, M. L.; Coffey, A. M.; Shchepin, R. V.; Waddell, K. W.; Shi, F.; Goodson, B. M.; Warren, W. S.; Chekmenev, E. Y. Microtesla SABRE Enables 10% Nitrogen-15 Nuclear Spin Polarization. *J. Am. Chem. Soc.* **2015**, *137*, 1404−1407.
(27) Zhivonitko, V. V.; Skovpin, I. V.; Koptyug, I. V. Strong ^{31}P Nuclear Spin Hyperpolarization Produced Via Reversible Chemical Interaction with Parahydrogen. *Chem. Commun.* **2015**, *51*, 2506−2509.
(28) Shchepin, R. V.; Truong, M. L.; Theis, T.; Coffey, A. M.; Shi, F.; Waddell, K. W.; Warren, W. S.; Goodson, B. M.; Chekmenev, E. Y. Hyperpolarization of "Neat" Liquids by NMR Signal Amplification by Reversible Exchange. *J. Phys. Chem. Lett.* **2015**, *6*, 1961−1967.
(29) Truong, M. L.; Theis, T.; Coffey, A. M.; Shchepin, R. V.; Waddell, K. W.; Shi, F.; Goodson, B. M.; Warren, W. S.; Chekmenev, E. Y. ^{15}N Hyperpolarization by Reversible Exchange Using SABRE-SHEATH. *J. Phys. Chem. C* **2015**, *119*, 8786−8797.
(30) Kiryutin, A. S.; Yurkovskaya, A. V.; Zimmermann, H.; Vieth, H.-M.; Ivanov, K. L. Complete Magnetic Field Dependence of SABRE-Derived Polarization. *Magn. Reson. Chem.* **2018**, *56*, 651−662.
(31) Theis, T.; Truong, M.; Coffey, A. M.; Chekmenev, E. Y.; Warren, W. S. LIGHT-SABRE Enables Efficient in-Magnet Catalytic Hyperpolarization. *J. Magn. Reson.* **2014**, *248*, 23−26.
(32) Pravdivtsev, A. N.; Yurkovskaya, A. V.; Vieth, H.-M.; Ivanov, K. L. RF-SABRE: A Way to Continuous Spin Hyperpolarization at High Magnetic Fields. *J. Phys. Chem. B* **2015**, *119*, 13619−13629.
(33) Pravdivtsev, A. N.; Skovpin, I. V.; Svyatova, A. I.; Chukanov, N. V.; Kovtunova, L. M.; Bukhtiyarov, V. I.; Chekmenev, E. Y.; Kovtunov, K. V.; Koptyug, I. V.; Hövener, J.-B. Chemical Exchange Reaction Effect on Polarization Transfer Efficiency in SLIC-SABRE. *J. Phys. Chem. A* **2018**, *122*, 9107−9114.
(34) Lindale, J. R.; Eriksson, S. L.; Tanner, C. P. N.; Zhou, Z.; Colell, J. F. P.; Zhang, G.; Bae, J.; Chekmenev, E. Y.; Theis, T.; Warren, W. S. Unveiling Coherently driven Hyperpolarization Dynamics in Signal Amplification by Reversible Exchange. *Nat. Commun.* **2019**, *10*, 395.
(35) Pravdivtsev, A. N.; Yurkovskaya, A. V.; Zimmermann, H.; Vieth, H.-M.; Ivanov, K. L. Transfer of SABRE-Derived Hyperpolarization to Spin-1/2 Heteronuclei. *RSC Adv.* **2015**, *5*, 63615−63623.
(36) Roy, S. S.; Stevanato, G.; Rayner, P. J.; Duckett, S. B. Direct Enhancement of Nitrogen-15 Targets at High-Field by Fast ADAPT-SABRE. *J. Magn. Reson.* **2017**, *285*, 55−60.
(37) Shchepin, R. V.; Jaigirdar, L.; Chekmenev, E. Y. Spin-Lattice Relaxation of Hyperpolarized Metronidazole in Signal Amplification by Reversible Exchange in Micro-Tesla Fields. *J. Phys. Chem. C* **2018**, *122*, 4984−4996.
(38) Theis, T.; Ortiz, G. X.; Logan, A. W. J.; Claytor, K. E.; Feng, Y.; Huhn, W. P.; Blum, V.; Malcolmson, S. J.; Chekmenev, E. Y.; Wang, Q.; et al. Direct and Cost-Efficient Hyperpolarization of Long-Lived Nuclear Spin States on Universal $^{15}N_2$-Diazirine Molecular Tags. *Sci. Adv.* **2016**, *2*, e1501438.
(39) Nonaka, H.; Hata, R.; Doura, T.; Nishihara, T.; Kumagai, K.; Akakabe, M.; Tsuda, M.; Ichikawa, K.; Sando, S. A Platform for Designing Hyperpolarized Magnetic Resonance Chemical Probes. *Nat. Commun.* **2013**, *4*, 2411.
(40) Bales, L.; Kovtunov, K. V.; Barskiy, D. A.; Shchepin, R. V.; Coffey, A. M.; Kovtunova, L. M.; Bukhtiyarov, A. V.; Feldman, M. A.; Bukhtiyarov, V. I.; Chekmenev, E. Y.; et al. Aqueous, Heterogeneous Parahydrogen-Induced ^{15}N Polarization. *J. Phys. Chem. C* **2017**, *121*, 15304−15309.
(41) McCormick, J.; Korchak, S.; Mamone, S.; Ertas, Y. N.; Liu, Z.; Verlinsky, L.; Wagner, S.; Glöggler, S.; Bouchard, L.-S. More Than 12% Polarization and 20 minute Lifetime of ^{15}N in a Choline

DOI: 10.1021/acs.jpclett.9b01505
J. Phys. Chem. Lett. 2019, 10, 4229−4236

Derivative Utilizing Parahydrogen and a Rhodium Nanocatalyst in Water. *Angew. Chem., Int. Ed.* **2018**, *57*, 10692−10696.
(42) Zhang, G.; Colell, J. F. P.; Glachet, T.; Lindale, J. R.; Reboul, V.; Theis, T.; Warren, W. S. Terminal Diazirines Enable Reverse Polarization Transfer from $^{15}N_2$ Singlets. *Angew. Chem., Int. Ed.* **2019**, DOI: 10.1002/anie.201904026.
(43) Shchepin, R. V.; Birchall, J. R.; Chukanov, N. V.; Kovtunov, K. V.; Koptyug, I. V.; Theis, T.; Warren, W. S.; Gelovani, J. G.; Goodson, B. M.; Shokouhi, S.; et al. Hyperpolarizing Concentrated Metronidazole $^{15}NO_2$ Group over Six Chemical Bonds with More Than 15% Polarization and 20 minute Lifetime. *Chem. - Eur. J.* **2019**, *25*, 8829−8836.
(44) Chukanov, N. V.; Kidd, B. M.; Kovtunova, L. M.; Bukhtiyarov, V. I.; Shchepin, R. V.; Chekmenev, E. Y.; Goodson, B. M.; Kovtunov, K. V.; Koptyug, I. V. A Versatile Synthetic Route to the Preparation of ^{15}N Heterocycles. *J. Labelled Compd. Radiopharm.* **2019**, DOI: 10.1002/jlcr.3699.
(45) Shchepin, R. V.; Barskiy, D. A.; Mikhaylov, D. M.; Chekmenev, E. Y. Efficient Synthesis of Nicotinamide-1-^{15}N for Ultrafast NMR Hyperpolarization Using Parahydrogen. *Bioconjugate Chem.* **2016**, *27*, 878−882.
(46) Shchepin, R. V.; Barskiy, D. A.; Coffey, A. M.; Feldman, M. A.; Kovtunova, L. M.; Bukhtiyarov, V. I.; Kovtunov, K. V.; Goodson, B. M.; Koptyug, I. V.; Chekmenev, E. Y. Robust Imidazole-$^{15}N_2$ Synthesis for High-Resolution Low-Field (0.05 T) ^{15}N hyperpolarized NMR Spectroscopy. *ChemistrySelect* **2017**, *2*, 4478−4483.
(47) Shen, K.; Logan, A. W. J.; Colell, J. F. P.; Bae, J.; Ortiz, G. X., Jr.; Theis, T.; Warren, W. S.; Malcolmson, S. J.; Wang, Q. Diazirines as Potential Molecular Imaging Tags: Probing the Requirements for Efficient and Long-Lived SABRE-Induced Hyperpolarization. *Angew. Chem., Int. Ed.* **2017**, *56*, 12112−12116.
(48) Wang, J.; Sánchez-Roselló, M.; Aceña, J. L.; del Pozo, C.; Sorochinsky, A. E.; Fustero, S.; Soloshonok, V. A.; Liu, H. Fluorine in Pharmaceutical Industry: Fluorine-Containing Drugs Introduced to the Market in the Last Decade (2001−2011). *Chem. Rev.* **2014**, *114*, 2432−2506.
(49) Ojima, I. *Fluorine in Medicinal Chemistry and Chemical Biology*; Wiley-Backwell, 2009.
(50) Shchepin, R. V.; Goodson, B. M.; Theis, T.; Warren, W. S.; Chekmenev, E. Y. Toward Hyperpolarized ^{19}F Molecular Imaging Via Reversible Exchange with Parahydrogen. *ChemPhysChem* **2017**, *18*, 1961−1965.
(51) Chukanov, N. V.; Salnikov, O. G.; Shchepin, R. V.; Svyatova, A.; Kovtunov, K. V.; Koptyug, I. V.; Chekmenev, E. Y. ^{19}F Hyperpolarization of ^{15}N-3-^{19}F-Pyridine Via Signal Amplification by Reversible Exchange. *J. Phys. Chem. C* **2018**, *122*, 23002−23010.
(52) Buckenmaier, K.; Rudolph, M.; Back, C.; Misztal, T.; Bommerich, U.; Fehling, P.; Koelle, D.; Kleiner, R.; Mayer, H. A.; Scheffler, K.; et al. SQUID-Based Detection of Ultra-Low-Field Multinuclear NMR of Substances Hyperpolarized Using Signal Amplification by Reversible Exchange. *Sci. Rep.* **2017**, *7*, 13431.
(53) Olaru, A. M.; Robertson, T. B. R.; Lewis, J. S.; Antony, A.; Iali, W.; Mewis, R. E.; Duckett, S. B. Extending the Scope of ^{19}F Hyperpolarization through Signal Amplification by Reversible Exchange in MRI and NMR Spectroscopy. *ChemistryOpen* **2018**, *7*, 97−105.
(54) Theis, T.; Ariyasingha, N. M.; Shchepin, R. V.; Lindale, J. R.; Warren, W. S.; Chekmenev, E. Y. Quasi-Resonance Signal Amplification by Reversible Exchange. *J. Phys. Chem. Lett.* **2018**, *9*, 6136−6142.
(55) DeVience, S. J.; Walsworth, R. L.; Rosen, M. S. Preparation of Nuclear Spin Singlet States Using Spin-Lock Induced Crossing. *Phys. Rev. Lett.* **2013**, *111*, 173002.
(56) Shchepin, R. V.; Jaigirdar, L.; Theis, T.; Warren, W. S.; Goodson, B. M.; Chekmenev, E. Y. Spin Relays Enable Efficient Long-Range Heteronuclear Signal Amplification by Reversible Exchange. *J. Phys. Chem. C* **2017**, *121*, 28425−28434.
(57) Truong, M. L.; Shi, F.; He, P.; Yuan, B.; Plunkett, K. N.; Coffey, A. M.; Shchepin, R. V.; Barskiy, D. A.; Kovtunov, K. V.; Koptyug, I. V.; et al. Irreversible Catalyst Activation Enables Hyperpolarization and Water Solubility for NMR Signal Amplification by Reversible Exchange. *J. Phys. Chem. B* **2014**, *18*, 13882−13889.
(58) Eshuis, N.; Aspers, R. L. E. G.; van Weerdenburg, B. J. A.; Feiters, M. C.; Rutjes, F. P. J. T.; Wijmenga, S. S.; Tessari, M. Determination of Long-Range Scalar $^1H-^1H$ Coupling Constants Responsible for Polarization Transfer in SABRE. *J. Magn. Reson.* **2016**, *265*, 59−66.
(59) Theis, T.; Feng, Y.; Wu, T.; Warren, W. S. Composite and Shaped Pulses for Efficient and Robust Pumping of Disconnected Eigenstates in Magnetic Resonance. *J. Chem. Phys.* **2014**, *140*, 014201.
(60) Shchepin, R. V.; Barskiy, D. A.; Coffey, A. M.; Goodson, B. M.; Chekmenev, E. Y. NMR Signal Amplification by Reversible Exchange of Sulfur-Heterocyclic Compounds Found in Petroleum. *ChemistrySelect* **2016**, *1*, 2552−2555.
(61) Iali, W.; Roy, S. S.; Tickner, B. J.; Ahwal, F.; Kennerley, A. J.; Duckett, S. B. Hyperpolarising Pyruvate through Signal Amplification by Reversible Exchange (SABRE). *Angew. Chem., Int. Ed.* **2019**, DOI: 10.1002/anie.201905483.
(62) Eshuis, N.; Aspers, R. L. E. G.; van Weerdenburg, B. J. A.; Feiters, M. C.; Rutjes, F. P. J. T.; Wijmenga, S. S.; Tessari, M. 2D NMR Trace Analysis by Continuous Hyperpolarization at High Magnetic Field. *Angew. Chem., Int. Ed.* **2015**, *54*, 14527−14530.

DOI: 10.1021/acs.jpclett.9b01505
J. Phys. Chem. Lett. 2019, 10, 4229−4236